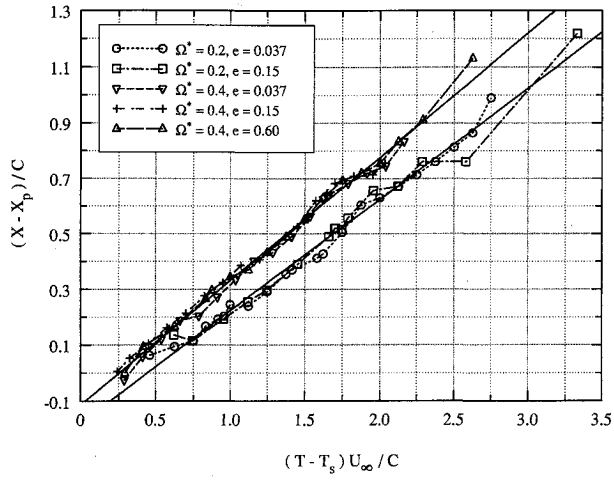

Fig. 4 Downstream convection of the dynamic stall vortex. Solid lines represent the least-squares line fit to data.

of leading-edge separation might be expected to be insensitive to the motion history, as is resported here. This is consistent with the constant pitch rate, inviscid flow, lift-curve slope results in Ref. 4 which indicate that at high enough pitch rates motion history effects will saturate. We should mention that in all of the cases studied here, the acceleration period was short enough that it ended before the onset of leading-edge separation. Reference 10 further suggests that initial acceleration effects may become important for a combination of low pitch rate Ω^* and long acceleration period e.

We note that the results presented here only address the timing of the various events in the flowfield development. We do not know at this time how other important quantities such as the surface pressure gradient, surface vorticity flux, and the integrated load on the airfoil are affected as we change the acceleration period. These questions are currently being addressed by computing the flows discussed here using a two-dimensional Navier-Stokes solver. Preliminary computational results[11] corroborate the present findings.

Acknowledgments

This work was supported by the Air Force Office of Scientific Research Grants AFOSR-89-0417 and AFOSR-89-0130. Charles Gendrich is gratefully acknowledged for his help with the preparation of the manuscript.

References

[1]McCroskey, W. J., "Unsteady Airfoils," *Annual Review of Fluid Mechanics,* Vol. 14, 1982, pp. 285–311.

[2]Carr, L. W., "Progress in Analysis and Prediction of Dynamic Stall," *Journal of Aircraft,* Vol. 25, No. 1, 1988, pp. 6–17.

[3]Francis, M. S., and Keesee, J. E., "Airfoil Dynamic Stall Performance with Large-Amplitude Motions," *AIAA Journal,* Vol. 23, No. 11, 1985, pp. 1653–1659.

[4]Jumper, E. J., Shreck, S. J., and Dimmick, R. L., "Lift-Curve Characteristics for an Airfoil Pitching at Constant Rate," *Journal of Aircraft,* Vol. 24, No. 10, 1987, pp. 680–687.

[5]Lorber, P. F., and Carta, F. O., "Airfoil Dynamic Stall at Constant Pitch Rate and High Reynolds Number," *Journal of Aircraft,* Vol. 25, No. 6, 1988, pp. 548–556.

[6]Visbal, M. R., "On the Formation and Control of the Dynamic Stall Vortex on a Pitching Airfoil," AIAA Paper 91-0006, Jan. 1991.

[7]Ghia, K. N., Yang, J., Osswald, G. A., and Ghia, U., "Study of the Dynamic Stall Mechanism Using Simulation of Two-Dimensional Navier-Stokes Equations," AIAA Paper 91-0546, Jan. 1991.

[8]Acharya, M., and Metwally, M. H., "Unsteady Pressure Field and Vorticity Production over a Pitching Airfoil," *AIAA Journal,* Vol. 30, No. 2, 1992, pp. 403–411.

[9]Shih, C., Lourenco, L., Van Dommelen, L., and Krothapalli, A., "Unsteady Flow Past an Airfoil Pitching at Constant Rate," *AIAA Journal,* Vol. 30, No. 5, 1992, pp. 1153–1161.

[10]Koochesfahani, M. M., Smiljanovski, V., and Brown, T. A., "Effect of Initial Acceleration on the Flow Development of the Flow Field of an Airfoil Pitching at Constant Rate," *Proceedings of NASA/AFOSR/ARO Workshop on Physics of Forced Unsteady Separation,* NASA Ames Research Center, April 17–19, 1990, NASA CP 3144, 1992, pp. 317–332.

[11]Gendrich, C. P., Koochesfahani, M. M., and Visbal, M. R., "Initial Acceleration Effects on the Flow Field Development around Rapidly Pitching Airfoils," AIAA Paper 93-0438, Jan. 1993.

Decay of Aircraft Vortices near the Ground

Milton E. Teske* and Alan J. Bilanin†
Continuum Dynamics, Inc., Princeton, New Jersey 08543
and
John W. Barry‡
U.S. Department of Agriculture Forest Service, Davis, California 95616

Introduction

In a review of the state of knowledge of aircraft vortices, Donaldson and Bilanin[1] include a discussion on the effects of atmospheric turbulence on the aging of vortex pairs. One of the models suggested may be written

$$\Gamma(t) = \Gamma_o \exp\left(-\frac{bqt}{s}\right) \tag{1}$$

where Γ is the vortex circulation strength as a function of time t, Γ_o the initial vortex circulation strength at $t = 0$, b the decay coefficient, q the ambient turbulence level, and s the aircraft semispan.

Donaldson and Bilanin[1] invoke simple arguments to suggest that the decay coefficient—out of ground effect—may take a value of 0.41. When details about the wakes of large aircraft were first investigated (in the early 1970s), more sophisticated models, using various techniques such as second-order closure of the Reynolds stress equations,[2] were developed with an eye toward examining this decay behavior. Recently, for a completely different reason, the problem of quantifying the decay coefficient has produced a sizable field study and data examination.

Discussion

Between 1985 and 1991, a series of aircraft flybys above tower grids instrumented with propeller anemometers produced a large data base on vortex motion near the ground.[3] These tests were performed jointly by the United States Department of Agriculture Forest Service and the United States Army at several sites in northern California (through Project WIND), and at Dugway Proving Ground, Utah. Anemometer tower grids recorded the ambient vertical velocity time histories as various aircraft repeatedly traversed normal to the grid. These digitized velocity traces produced an aircraft wake signature that could be used to infer the strength and lateral and vertical motion of the aircraft vortex pairs generating the traces. Table 1 summarizes the complete data set.

The location and strength of the vortices traversing the anemometer tower grid may be inferred by a least-squares analysis defining an error E as

$$E = \sum_{n=1}^{N} (w_n - \bar{w}_n)^2 \tag{2}$$

Received Nov. 12, 1992; revision received Jan. 15, 1993; accepted for publication Feb. 5, 1993. Copyright © 1993 by the American Institute of Aeronautics and Astronautics, Inc. All rights reserved.

*Senior Associate, P.O. Box 3073.
†President and Senior Associate, P.O. Box 3073.
‡Pesticide Specialist, Forest Pest Management, 2121C Second Street, Suite 102.

Table 1 Field study summary

Location	Aircraft	Ground cover	Flybys
Forest Hill	Bell 206B	Open field	18
	Ag Husky	Open field	31
	Bell 206B	Forest	36
	Ag Husky	Forest	35
Chico	Ag Cat	Almond orchard	40
	Hiller 12E	Almond orchard	60
Red Bluff	C-130	Downslope clearing	4
	Bell 206B	Downslope clearing	45
Dugway	F-4	Flat desert	15
	F-15	Flat desert	12
	F-16	Flat desert	14
Total			310

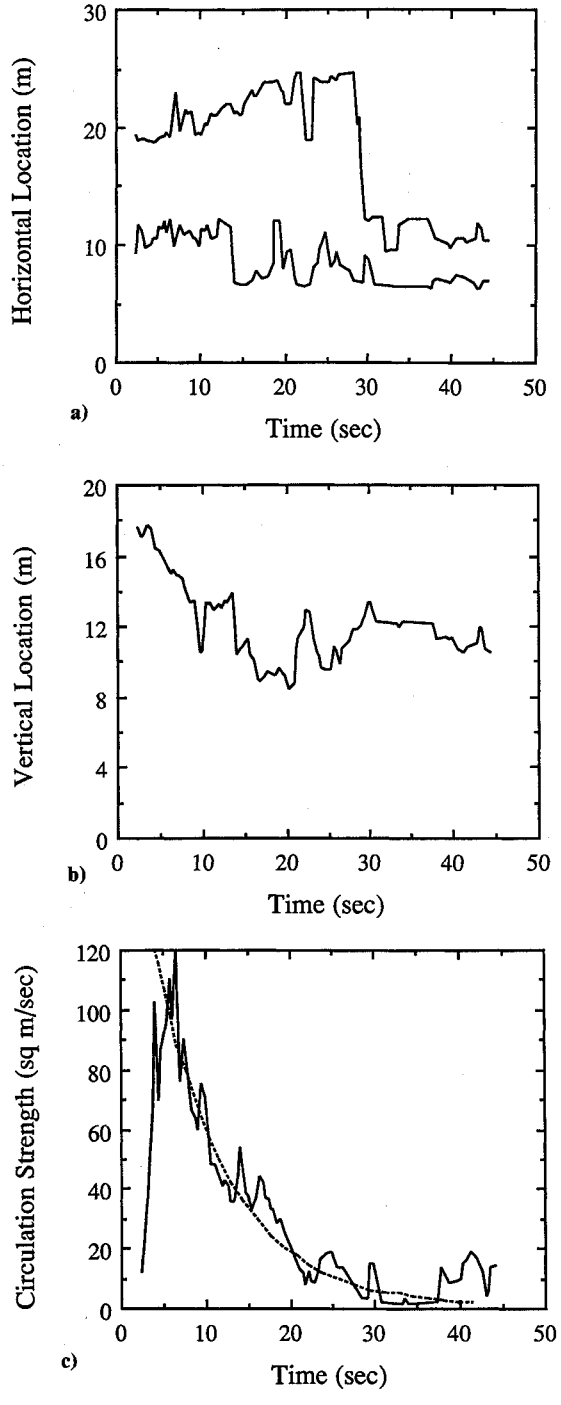

Fig. 1 Forest Hill run 68 algorithm results: a) horizontal location of the vortices; b) vertical location of the vortices; and c) vortex circulation strength. The vortex circulation curve fit is shown as the dashed curve in Fig. 1c.

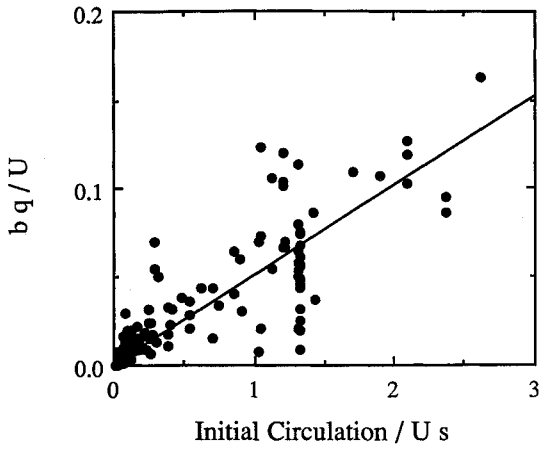

Fig. 2 Behavior of vortex decay [from Eq. (1)] with initial vortex circulation strength. The slope of the least-squares line is 0.051 with a correlation coefficient of $R^2 = 0.859$.

where the overbar denotes the data, and N is the total number of anemometers. Equation (2) is examined for each time increment of data. The vertical velocities w are determined by summing the contributions of the four vortices in the model (the two wing tip vortices and their images below the ground), written in vortex-centered coordinates as

$$v = \Gamma/2\pi R \tag{3}$$

where v is the vortex velocity magnitude and R is the radius from the vortex center. The need for spatial resolution positions the vortices horizontally and vertically relative to an arbitrarily chosen origin. Thus, in its simplest form, the minimization technique represented by Eq. (2) requires the resolution of three parameters: the vortex strength Γ and the horizontal and vertical positions of the vortex pair traversing the tower grid. Because aircraft wake physics are only approximated by the simple velocity law given in Eq. (3), the intent of the present analysis to seek a solution minimizing the error in the velocity predictions at all anemometer locations seems appropriate.

Most of the flybys were conducted in the early morning hours where stable atmospheric conditions existed. Where data are available, the Richardson number has been computed to be no more unstable than -0.20. Figure 1 illustrates a typical vortex pair trace, and the resulting curve fit to Eq. (1). Figure 2 displays all reduced data. Least squares through the data produces the line

$$bq/U_\infty = 0.051(\Gamma_o/U_\infty s) \tag{4}$$

with a correlation coefficient of $R^2 = 0.859$, where U_∞ is the flight speed of the aircraft. Substitution for the initial vortex strengths and the inferred ambient turbulence levels gives an average value of decay coefficient of $b = 1.66$ with a standard deviation of 2.25.

Vortical decay has been implemented into the aerial application models AGDISP[4] and FSCBG[5] with improved predictions in ground deposition and comparisons with data.

References

[1]Donaldson, C. duP., and Bilanin, A. J., "Vortex Wakes of Conventional Aircraft," AGARDograph No. 204, May 1975.

[2]Bilanin, A. J., Teske, M. E., and Williamson, G. G., "Vortex Interactions and Decay in Aircraft Wakes," *AIAA Journal*, Vol. 15, No. 2, 1977, pp. 250–260.

[3]Bilanin, A. J., Teske, M. E., Barry, J. W., and Ekblad, R. B., "Project WIND Anemometer Tower Flyby Data Reduction," *Proceedings of the 19th Conference on Agricultural and Forest Meteorology*, American Meteorological Society, Charleston, SC, 1989, pp. 188–201.

[4]Bilanin, A. J., Teske, M. E., Barry, J. W., and Ekblad, R. B., "AGDISP: The Aircraft Spray Dispersion Model, Code Development and Experimental Validation," *Transactions of the American Society of Agricultural Engineers*, Vol. 32, No. 1, 1989, pp. 327–334.

[5]Teske, M. E., Bowers, J. F., Rafferty, J. E., and Barry, J. W., "FSCBG: An Aerial Spray Dispersion Model for Predicting the Fate of Released Material Behind Aircraft," *Environmental Toxicology and Chemistry*, Vol. 12, No. 3, 1993, pp. 453–464.

Material Model for Composites Using Neural Networks

R. M. V. Pidaparti* and M. J. Palakal†
Purdue University, Indianapolis, Indiana 46202

Introduction

ADVANCED materials such as composites are being used in a variety of engineering applications. These composites exhibit complex behaviors such as anisotropy, microcracking, fiber breakage, etc. Constitutive equations are being developed to describe these complex behaviors using some mathematical rules and expressions based on either experimental data or a theory. The constitutive equations describe the relationship between stresses and strains. A new computational paradigm using Artificial Neural Network provides a fundamentally different approach to the derivation and representation of composite material behavior relationships. Neural network (NN) is a paradigm for computation and knowledge representation inspired by the neuronal architecture and operation of the brain.[1,2]

There have been considerable research efforts in different applications of NN: signal processing,[2] robotics,[3] structural analysis and design,[4] and pattern recognition[5,6] to name a few. Other related work in the use of NN for effective modeling of complex, highly nonlinear relationship among data sets can be found in Ref. 7. The resurgence of earlier research in NN has facilitated the development of a totally different approach to the derivation and representation of material behavior. With this new approach, the knowledge of the material's behavior is captured within the connections of a self-organizing NN that has been trained with experimental data. Recently, the stress-strain behavior of concrete material under the plane stress condition was modeled with a back-propagation (BP) neural network.[8]

A neural-network-based material model is developed as an alternative to mathematical modeling of composite material behavior. Neural-network-based modeling solutions are better than conventional methods, such as nonlinear regression analysis, etc., for handling unknown data sets, large dimensional data sets, and noisy data. In this Note, the nonlinear stress-strain behavior of $(\pm\theta)$ graphite-epoxy laminates under monotonic and cyclic loadings is modeled with a back-propagation neural network. The NN predicted stress-strain behavior is compared to the experimental data for both monotonic and cyclic loadings.

Neural-Network-Based Material Model

The underlying rationale for developing a neural-network-based material model is to train a back-propagation neural network to map the stress-strain relationship on the results of experimental data for a material. The trained network would contain sufficient information about the material behavior. This trained network could be qualified as a material model when the network is able to reproduce the trained experimental data and also the untrained experimental data for generalization. In general, the material behavior might be complex, exhibiting nonlinear characteristics in stress-strain behavior, anisotropy, fiber breakage, etc. As a first attempt, the neural network can also be based on traditional mathematical models if no experimental data is available. Since the material behavior of graphite-epoxy composites is highly nonlinear and exhibit stiffening and softening behavior for various fiber angles,[9] the input data to the network must have sufficient information about the material behavior.

Graphite-epoxy laminates were chosen as a first example of material modeling with neural network for composite materials. In the present study, a back-propagation neural network is developed for predicting the nonlinear stress-strain behavior of $(\pm\theta)$ graphite-epoxy laminates. More details regarding the BP learning algorithm can be found in Refs. 6-7. The BP network gives the input/output relation in the form of a functional fit for a set of data points. Currently there are no rules available in the literature for determining the NN architecture (as this question is under research). The architecture used in this study was based on empirical results. The back-propagation NN developed in this investigation has one input layer with three nodes, two middle layers with 17 processing elements each, and one output layer with one node (3- 17- 17- 1) (see Fig. 1a). The input parameters chosen in this study are fiber angle, initial stress, and incremental stress, and the output is the total strain. There might be other possibilities: for example, the input parameters can be fiber angle, initial strain, and incremental strain, and the output can be the total stress. The present results are assumed to be stress controlled, i.e., stress as input and strain as output. There are two main phases involved in this neural-network-based modeling: learning and testing.

Learning

Learning or training involves presenting the network with the experimental data so that it correctly reproduces the total strain when presented with the current states of stress and incremental stress by modifying its weights. Learning also involves the transformation of the stress-strain data into the network as input and output, and presenting this information repeatedly to the network. It is discovered that an effective way to train the neural network is to present the data in normalized form, In this study, the fiber-angle values in the data set were normalized between 1.0 and 12.0 while

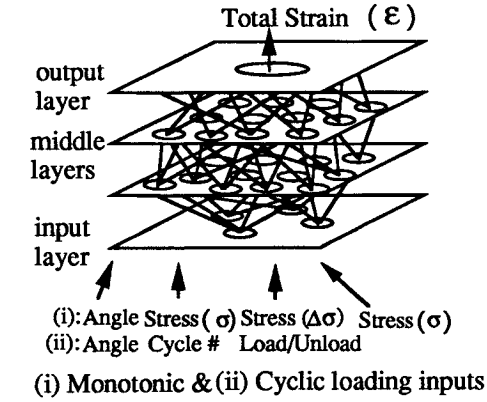

Fig. 1 Neural network representation for monotonic and cyclic stress-strain behavior: a) architecture and b) typical stress-strain behavior.

Received June 26, 1992; revision received Feb. 8, 1993; accepted for publication Feb. 28, 1993. Copyright © 1993 by R. M. V. Pidaparti. Published by the American Institute of Aeronautics and Astronautics, Inc., with permission.

*Associate Professor, Department of Mechanical Engineering, 723 West Michigan Street. Member AIAA.

†Assistant Professor, Department of Computer Science, 723 West Michigan Street.